World Academy of Science, Engineering and Technology
International Journal of Materials and Metallurgical Engineering
Vol:17, No:7, 2023

Optimization of Thermopile Sensor Performance of Polycrystalline Silicon Film

Li Long, Thomas Ortlepp

Open Science Index, Materials and Metallurgical Engineering Vol:17, No:7, 2023 publications.waset.org/10013161.pdf

Abstract—A theoretical model for the optimization of thermopile sensor performance is developed for thermoelectric-based infrared radiation detection. It is shown that the performance of polycrystalline silicon film thermopile sensor can be optimized according to the thermoelectric quality factor, sensor layer structure factor and sensor layout shape factor. Based on the properties of electrons, phonons, grain boundaries and their interactions, the thermoelectric quality factor of polycrystalline silicon is analyzed with the relaxation time approximation of Boltzmann transport equation. The model includes the effects of grain structure, grain boundary trap properties and doping concentration. The layer structure factor of sensor is analyzed with respect to infrared absorption coefficient. The effect of layout design is characterized with the shape factor, which is calculated for different sensor designs. Double layer polycrystalline silicon thermopile infrared sensors on suspended support membrane have been designed and fabricated with a CMOS-compatible process. The theoretical approach is confirmed with measurement results.

Keywords—Polycrystalline silicon film, relaxation time approximation, specific detectivity, thermal conductivity, thermopile infrared sensor.

I. Introduction

POLYCRYSTALLINE silicon is widely used in the manufacture of thermopile infrared sensor due to its compatibility to CMOS process. Over the last years, a lot of effort has been made to improve the performance of thermopile sensors [1], [2], [3]. Thermopile sensors made with thin polycrystalline silicon film can achieve high specific detectivity for infrared radiation detection [4].

The detection performance of infrared sensor is characterized by specific detectivity (D^*) [3], [4]. The specific detectivity is determined by the thermal, electrical, thermoelectric, infrared optical properties of the film, film thickness and sensor layout geometry. It will be shown that, due to the two dimensional character of temperature profile of very thin film under infrared radiation, specific detectivity of sensor can be decomposed into the product of uncoupled thermoelectric quality factor (Y), film structure factor (S) and sensor layout shape factor (G_f). Thus, in the context of the detection of infrared radiation in polycrystalline silicon film thermopile sensor, the optimization of sensor performance can be recast as: the optimization of the Y factor in terms of grain size, trap parameters, and doping concentration of the film; the optimization of S factor in terms of infrared optical properties and thickness of the film; and the optimization of G_f factor in terms of sensor layout design.

This research was supported by BMWI projects of grant No. 49MF190037 and No. 49MF200129.

Li Long* and Thomas Ortlepp are with CiS Forschungsinstitut für Mikrosensorik GmbH, Konrad-Zuse-Str. 14, D-99099 Erfurt, Germany (*Corresponding author, e-mail: llong@cismst.de, tortlepp@cismst.de).

The thermoelectric quality factor, the Y factor, is introduced to effectively characterize the contribution of thermal and thermoelectric properties of sensing materials to thermopile-based infrared sensors (Section II). The Y factor is determined by the transport properties of charge carriers and phonons of semiconductor thermoelectric material. In this paper an approach is presented to model the combined contribution of phonons and charge carriers in polycrystalline semiconductors on a microscopic level and with the relaxation time approximation. Due to the Onsager reciprocal relation [1], the transport coefficients, namely electrical conductivity, thermal conductivity and Seebeck coefficient, are correlated and determined by the microscopic scattering of phonons and charge carriers [5]. Over the last years, a lot of research into the thermal and thermoelectric properties of semiconductor materials has been carried out. For polycrystalline silicon, the electronic transport (resistivity) was investigated with the Richardson thermionic emission and thermal field emission model of grain boundaries [6], [7]. The thermal property of polycrystalline silicon has been investigated with the Boltzmann transport equation of phonons [8]. Recent investigation shown that the power factor can be improved in nanocrystalline silicon [9], which can be explained by the energy filtering effect of potential barriers of the grain boundaries of the nanocrystalline material.

In this paper, the thermoelectric properties of polycrystalline silicon are studied with the relaxation time approximation of Boltzmann transport equation for both phonon and charge carrier scattering simultaneously. The polycrystalline silicon is modeled as crystallites combined with grain boundaries. For the crystallites, phonon transport will be analyzed with the approach of [8] and [10], whereas charge carrier transport will be analyzed with the approach of [11] for an Si-Ge alloy. For grain boundaries, defects caused by incomplete atomic bonding and disordered material in the grain boundary result in trapping states that reduce the number of carriers and create space charge regions in the crystalline grains [6]. The resulting potential barrier at the grain boundary scatters the carriers. For thermal conductivity due to phonon scattering, the model of [8] is adopted, where different scattering mechanisms for thermal transport (Section III-A) are taken into account. For thermoelectric properties due to charge carrier scattering, the potential barrier model of nanocrytallite in [9] is extended to include all scattering mechanisms inside the grains and potential barrier scatterings caused by both grain boundaries and grain boundary traps induced depletion (Section III-B). The approach and related parameters are described in [12]. Thus, a unified transport model for both phonons and charge

Open Science Index, Materials and Metallurgical Engineering Vol:17, No:7, 2023 publications.waset.org/10013161.pdf

carriers is obtained.

A theoretical formulation for the optimization of thermopile sensor performance, both static and dynamical properties, is presented in Section II for thermoelectric-based infrared radiation detection. The two dimensional character of temperature profile of thin film is utilized to decouple the contributions of material properties, film structure, and sensor layout design to the performance. The theoretical approach for the calculation of thermal and thermoelectric transport parameters is shown in Section III. A systematic simulation of Y factor for n-type polycrystalline silicon is performed in Section IV-A, and a brief simulation is presented for p-type polycrystalline silicon in Section IV-B. It is shown that for polycrystalline silicon higher Y factor can be achieved than that of crystalline silicon. It is also shown that higher doping concentration results in higher Y factor (although the Seebeck coefficient is getting smaller). The film structure optimization is presented in Section V. The time constant is discussed in Section VI. The layout design optimization is presented in Section VII. In Ssection VIII the technology steps and measurement results of double layer polycrystalline silicon thermopile infrared sensor on a suspended support membrane are presented. The measured prototyping performance agree well with the model developed. Finally, the approach is discussed and summarized in Section IX.

II. Performance of Infrared Thermopile Device

Thermopile sensor consists a number of thin thermopile strips (long strips of polycrystalline silicon film) on a support membrane encompassed with heat sink. The strips are so arranged in support membrane that each strip has one end connected to the heat sink. For infrared radiation detection, there are two important quality specifications for the sensor, i.e. the specific detectivity for static response and the time constant for dynamical response. For polycrytalline silicon infrared sensor the passive support membrane has much smaller thermal conductivity than that of active polycrystalline silicon film. Therefore, the influence of support membrane to the static response of the sensor is negligible, but its influence to the dynamical response is big due to its additional thermal capacitance.

A. Static Response

The specific detectivity of infrared sensor is defined as [4]

$$D^* = \frac{\sqrt{A\Delta f}}{V_n/R_s} \tag{1}$$

where A is the active area of the sensor, Δf is the frequency bandwidth, and V_n is the noise voltage. R_s is the responsivity, which is defined as the output signal per input infrared radiation power. The temperature distribution of thin film is approximately two dimensional. Further, because the thermopile strips are connected with one end to a heat sink and the the thermal conductivities of support membrane and separation layers are much smaller than that of polycrystalline silicon film, the heat flow inside each thermopile strip is approximately one-dimensional. For infrared thermopile sensor based on thermoelectric effect, the performance can be analyzed in a theoretical manner by investigating a thermopile structure comprising a single thin polycrystalline silicon film. In the following, the infrared absorption coefficient is denoted as λ, the reflectance of the surface as R, the thermal conductivity as κ, the electrical resistivity as ρ, and the Seebeck coefficient as α. The thin film thickness is t, it consists of n rectangular thermopile strips of lengths l_i, widths w_i, and the gaps between neighboring strips g_i, where i is from 1 to n. The infrared power density P is incident perpendicular to the sensor. One end of the thermopile strip is connected to heat sink of constant temperature T_0. The other end and both surfaces are thermal floating. The resulted temperature difference in thermopile strip induces a Seebeck voltage as sensing signal. There are two different ways to take electrical signal from the thermopile strip. Sensor with signal from the whole thermopile strip is defined here as type I sensor. Sensor with signal from a part of the thermopile strip is defined as type II sensor, where the signal part is between a point of strip and the heat sink with length p_i being smaller than l_i.

Thermopile sensor is composed of a lot of thermopile strips with one end contacted the common heat sink. All strips are electrically connected in series so that the output signal is the constructive sum of all n signals. For type I sensor, the temperature difference induced by the infrared radiation between both ends of thermopile strip i is

$$\Delta T_i = \frac{(1-R)(1-e^{-\lambda t})P l_i A_i}{2\kappa t w_i} \tag{2}$$

where $A_i = l_i w_i$ is the area of strip i. Here, the infrared absorption of the possible medium between the strips, and the heat flow between the neighboring strips are neglected. The responsivity of sensor is therefore

$$R_s = \frac{\alpha \sum_{i=1}^{n} \Delta T_i}{PA} \tag{3}$$

where the area is $A = \sum_{i=1}^{n} l_i(w_i + g_i)$. The noise voltage is

$$V_n = \sqrt{4kT\rho\frac{\Delta f}{t}\sum_{i=1}^{n}\frac{l_i}{w_i}} \tag{4}$$

where k is the Boltzmann constant and T the temperature.

The specific detectivity characterizing the static response is therefore

$$D^* = \frac{\alpha}{\kappa\sqrt{kT\rho}} \frac{(1-R)(1-e^{-\lambda t})}{\sqrt{t}} \frac{\sum_{i=1}^{n} l_i^2}{4\sqrt{A\sum_{i=1}^{n}\frac{l_i}{w_i}}} \tag{5}$$

It can be seen that, for this simplified thermopile sensor model, the thermoelectric properties, the infrared optical properties, and the sensor layout design are decoupled. That is, its specific detectivity can be expressed as the product of three factors: the thermoelectric quality factor, the layer structure factor and the layout shape factor.

By defining the thermoelectric quality factor (Y factor) as

$$Y = \frac{\alpha}{\kappa\sqrt{kT\rho}} \tag{6}$$

Open Science Index, Materials and Metallurgical Engineering Vol:17, No:7, 2023 publications.waset.org/10013161.pdf

the layer structure factor (S factor) as

$$S = \frac{(1-R)(1-e^{-\lambda t})}{\sqrt{t}} \tag{7}$$

and the layout shape factor (G_f factor) for type I sensor as

$$G_f = \frac{\sum_{i=1}^{n} l_i^2}{4A\sqrt{\sum_{i=1}^{n} \frac{l_i}{w_i}}} \tag{8}$$

one obtains the specific detectivity as a combined effect of the above factors

$$D^* = YSG_f\sqrt{A} \tag{9}$$

Knowing the Y factor, one can easily estimate the specific detectivity of sensor. For more realistic multilayer infrared thermopile sensor, there will be some small deviation because the Y factor and the S factor can be weakly coupled. Nevertheless, it will be shown that the approach approximates the thin film sensor very well (Section VIII). The specific detectivity can therefore be optimized independently for these three factors. Therefore the contribution of thermoelectric material properties to D^* are summarized in a single Y factor. For thermoelectric material the conventionally employed characteristic parameter is the ZT factor [1]. It can be seen that a relation exists between these two parameters

$$Y = \sqrt{\frac{kZT}{\kappa}} \tag{10}$$

Nevertheless, the introduced Y factor better characterizes the thermal and thermoelectric properties of sensing material for infrared detection, because it contributes to the specific detectivity in a directly proportional manner. Further, the contribution of film layer structure is characterized by the S factor, which is determined by the infrared optical properties and film thickness. The contribution of sensor geometrical layout structure can be characterized by the G_f factor, which is determined by the configuration of thermopile strip lengths and widths. Similarly, it can be shown that the G_f factor of type II sensor is

$$G_f = \frac{\sum_{i=1}^{n} p_i(2l_i - p_i)}{4A\sqrt{\sum_{i=1}^{n} \frac{p_i}{w_i}}} \tag{11}$$

B. Dynamic Response

The dynamical response of sensor to transient infrared power can be approximately studied with a square membrane of polycrystalline silicon film of side length a. The thermal conductivity, specific heat capacity, mass density and thickness of polycrystalline silicon film are denoted as κ, c, ρ, and t respectively. The dynamical response is an exponential function with time constant τ, which is determined by the thermal resistance and thermal capacitance of the membrane. Defining the center thermal resistance for heat spreading to the edge (heat sink) as the ratio of temperature increase of the center of membrane $\Delta T(c)$ to the infrared power density P as

$$R_{th}^c = \frac{\Delta T(c)}{P} \tag{12}$$

and neglecting the blackbody radiation of membrane, one gets R_{th}^c for square membrane as

$$R_{th}^c = \frac{1}{4\kappa t}\left(1 - \frac{16}{\pi^3}\sum_{i=0}^{\infty} \frac{(-1)^k}{(2k+1)^3 cosh(\frac{(2k+1)\pi}{2})}\right) \tag{13}$$

The effective thermal resistance for the time constant will be

$$R_{th} = \frac{p}{4\kappa t} \tag{14}$$

where p is a constant factor. With ANSYS simulation, it is determined as $p = 0.24$. The time constant of the membrane is then

$$\tau = p\frac{c\rho A}{4\kappa} \tag{15}$$

For real thermopile sensor realized on a passive support membrane, the time constant will be influenced by this additional passive membrane. Although the thermal conductivity of passive membrane is small, its thermal capacitance will contribute to the time constant. If the specific heat capacity, mass density and thickness of the passive membrane are denoted as c_a, ρ_a, and t_a respectively, the total time constant can be approximated as

$$\tau = p\frac{c\rho A}{4\kappa}\left(1 + \frac{c_a\rho_a t_a}{c\rho t}\right) \tag{16}$$

In experiment rise time t_r (10% to 90%) is normally characterized, which is $t_r = ln(9)\tau \approx 2.2\tau$.

III. Thermal Conductivity and Thermoelectric Properties Modeling

Scattering at imperfections induces nonequilibrium distributions of phonons and charge carriers that hinder the transport of heat flux and charge current, respectively. The distribution functions obey the Boltzmann equation, which is a nonlinear differential equation. For small driving force, which is the case for most of the regime interesting for the thermoelectric detection of infrared radiation, a near-equilibrium solution can be obtained by using the relaxation time approximation. The polycrystalline silicon can be approximately modeled as crystalline silicon combined with grain boundary. Due to the highly stochastic grain distribution, scattering at different grains is incoherent and independent. As an approximation, the mean grain size is used to represent the real grain size distribution. In the following, the relaxation time approximation of the semiclassical description of phonon and charge carrier scattering is therefore applied to the transport problem.

A. Thermal Conductivity Due to Phonons

The thermal conductivity of semiconductors κ consists of the contributions of both types of charge carriers, κ_J for electrons and holes, which are treated in thermoelectric model [12], as well as the contribution of lattice vibrations κ_L. For silicon, the major contribution of lattice vibration scattering stems from one longitudinal and two transverse acoustic phonon bands, whereas the contribution of optical phonons

Open Science Index, Materials and Metallurgical Engineering Vol:17, No:7, 2023 publications.waset.org/10013161.pdf

can be neglected. Thus, the thermal conductivity κ_L for silicon can be expressed as:

$$\kappa_L = \frac{1}{3}\frac{k}{2\pi^2}(\frac{kT}{\hbar})^3 \sum_{j=L,TO,TU} \frac{1}{v_j} \int_0^{\frac{\theta_j}{T}} \tau_j \frac{x^4 e^x}{(e^x-1)^2} dx \quad (17)$$

where j is over longitudinal (L) and low and high frequency transverse (TO and TU) phonon modes, which contribute independently to the thermal transport. $x = \frac{\hbar\omega}{kT}$ is the reduced phonon energy for phonon frequency ω. v_j and τ_j (j stand for L, TO and TU) are the velocity and relaxation time of corresponding phonon modes, respectively. Further, the parameters θ_j and v_j are given in [8] and [13]. For each phonon mode j, there are various scattering processes i that can be combined according to Matthiessen's rule

$$\tau_j^{-1} = \sum_i \tau_{j,i}^{-1} \quad (18)$$

For doped polycrystalline silicon, the following phonon scattering processes are taken into account. Most parameters for phonon scattering are adopted from empirical values of literature [8].

1) Rayleigh scattering of impurities: The scattering of phonons at impurities exhibits an ω^4 dependence

$$\frac{1}{\tau_{j,I}} = D\omega^4 \quad (19)$$

Since the scattering of phonons at impurities is more involved than only the mass deficit of impurities introduced to the lattice, empiric values will be used in this work for the parameter D. For phosphorus, it is $4.2 \times 10^{-70} N_D\,[s^3]$, for boron $6.3 \times 10^{-70} N_A\,[s^3]$, where N_D and N_A are the donor and acceptor concentrations, respectively [8].

2) Phonon scattering: For different phonon modes, the relaxation times are [13]

$$\frac{1}{\tau_{TO,P}} = B_{TO}\omega T^4 \quad (20)$$

$$\frac{1}{\tau_{TU,P}} = B_{TU}\frac{\omega^2}{sinh(\frac{\hbar\omega}{kT})} \quad (21)$$

$$\frac{1}{\tau_{L,P}} = B_L\omega^2 T^3 \quad (22)$$

where $B_{TO} = 9.3 \times 10^{-13}\,K^{-4}$, $B_{TU} = 5.5 \times 10^{-18}\,s$ and $B_L = 2.0 \times 10^{-24}\,sK^{-3}$, respectively [13].

3) Grain boundary scattering: For polycrystalline silicon films, the effect of the grain boundaries should be taken into account. The relaxation time of the phonon scattering at grain boundaries can be modeled as [8]

$$\frac{1}{\tau_{j,G}} = \frac{v_s}{d}\frac{1-p(\omega)}{1+p(\omega)} \quad (23)$$

where d is the grain size and $p(\omega)$ is the probability of specular reflection

$$p(\omega) = \exp(-\pi(\frac{2\eta_g\omega}{v_s})^2) \quad (24)$$

where $\eta_g = 0.05\,nm$ is the grain boundary roughness factor used for polycrystalline silicon films in this paper.

B. Thermoelectric Properties Due to Charge Carriers

Since both the charge carrier concentration and scattering contribute to the transport properties of charge carriers, the relaxation time model of polycrystalline silicon is adopted [12]. The ionized impurity scattering, acoustic phonon scattering, optical phonon scattering, neutral impurity scattering, grain boundary potential barrier scattering and trap induced concentration reduction are taken into account. The model and parameters for the contribution of charge carrier scattering to thermal and thermoelectric properties are given in [12].

IV. Optimization of Y Factor

It was observed that deposition, doping and annealing affect the structural and electrical properties of polycrystalline silicon film [14]. Grain size, trap density and trap distribution can all be modified by the processing conditions. Apart from the optimization of the geometrical design, it is therefore also possible to improve the specific detectivity of thermopile infrared sensors by modifying the processing conditions of the polycrystalline silicon film (Section II). Thus, the effects of grain size, trap density, doping concentration, and temperature on the Y factor are analyzed with the approach presented in Section III.

A. n-Type Polycrystalline Silicon Film

For donor doping concentration from $10^{17}\,cm^{-3}$ to $10^{20}\,cm^{-3}$, the Y factors are calculated for temperatures ranging from $260\,K$ to $360\,K$ for n-type polycrystalline silicon (Fig. 1). As default parameters, a mean grain size of $100\,nm$, a trap density of $2 \times 10^{12}\,cm^{-2}$, and a trap energy position of $0.42\,eV$ below the conduction band edge [15] are assumed. It can be seen that the Y factor is better for heavily doped materials.

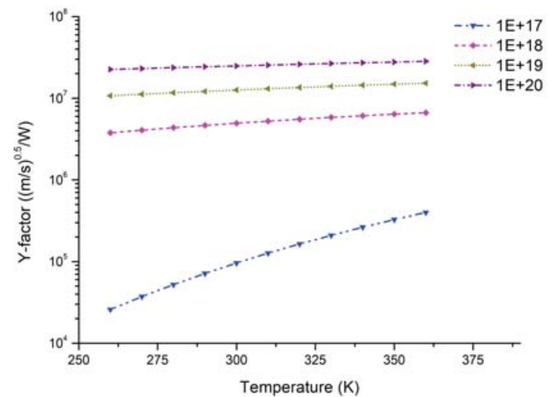

Fig. 1 The Y factor as a function of temperature for four different doping concentrations in n-doped polycrystalline silicon.

For comparison, the Y factors of the corresponding crystalline silicon are shown in Fig. 2. It can be seen that the Y factor of polycrystalline silicon is a bit better than that of crystalline silicon for high doping concentrations.

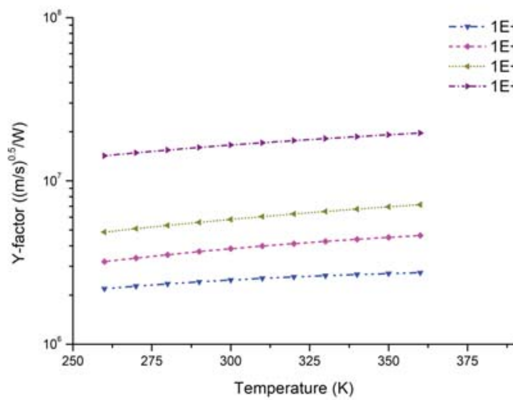

Fig. 2 The Y factor as a function of temperature for four different doping concentrations in n-doped crystalline silicon

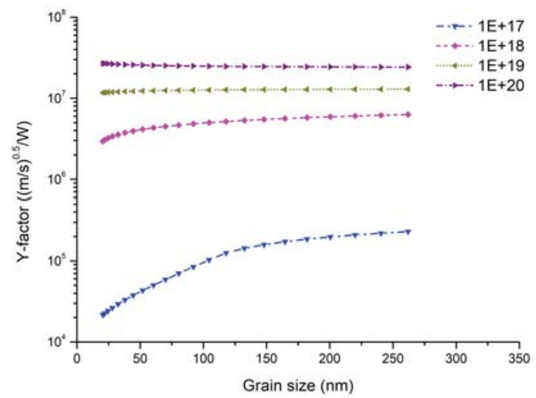

Fig. 4 The Y factor as a function of mean grain size for four different doping concentrations at $300K$ in n-doped polycrystalline silicon

For the optimization of processing conditions, the effect of the mean grain size is analyzed at $300\,K$ for mean grain sizes ranging from $20\,nm$ to $260\,nm$. Here, the default trap parameters are used. It has been seen that [12] smaller grain sizes cause bigger Seebeck coefficient for polycrystalline silicon film. Although the Seebeck coefficient is high for weakly doped polycrystalline silicon film, the electrical conductivity is bigger for higher doping concentrations. At the same time, it is observed (Fig. 3) that the thermal conductivity is small for heavily doped silicon film. The Y factor as a function of mean grain size is plotted in Fig. 4. At low doping concentrations ($10^{17}\,cm^{-3}$), the Y factor increases with the grain size for small grains before it reaches a saturation value. Whereas at high doping concentration the Y factor decreases slightly with the grain size. This behavior is due to the concurrent interaction between phonon scattering (which is beneficial for smaller grains) and charge carrier scattering (which is harmful for smaller grains).

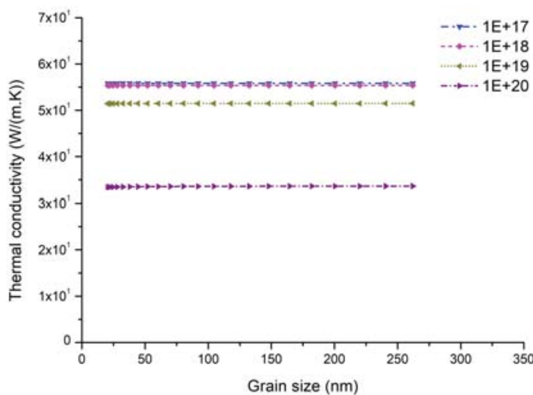

Fig. 3 The thermal conductivity as a function of mean grain size for four different doping concentrations at $300K$ in n-doped polycrystalline silicon

In the same way, one can investigate the effects of trap density (Fig. 5) on the Y factor at $300\,K$. The trap density can be effectively modified with annealing, whereas the trap energy level position may depend upon the grain boundary structure. Here the grain size is $100\,nm$. Furthermore, when changing the trap density, the other parameters are kept fixed at its default value. It can be seen that, if the doping concentration is higher than a critical value, the Y factor saturates, i.e. it does not change with the trap density. Furthermore, in these cases, the effect of traps is small and almost independent of trap density.

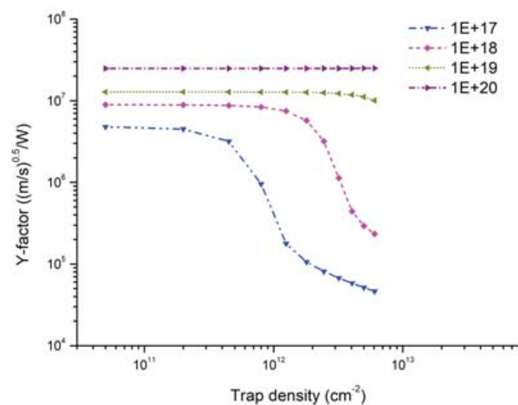

Fig. 5 The Y factor as a function of grain boundary trap density for four different doping concentrations at $300K$ in n-doped polycrystalline silicon

B. p-Type Polycrystalline Silicon Film

The same analyses have been performed for p-type polycrystalline silicon materials. For acceptor doping concentration ranging from $10^{17}\,cm^{-3}$ to $10^{20}\,cm^{-3}$, the resulting Y factors (Fig. 6) are calculated at $300\,K$ for mean grain sizes ranging from $20\,nm$ to $260\,nm$. A trap density of $2 \times 10^{12}\,cm^{-2}$, and a trap energy position at $0.38\,eV$ ([6], [16]) above the valence band edge are supposed here. It can also be seen that the Y factor, which combines all scattering and trapping effects, is also better for heavily doped film.

Open Science Index, Materials and Metallurgical Engineering Vol:17, No:7, 2023 publications.waset.org/10013161.pdf

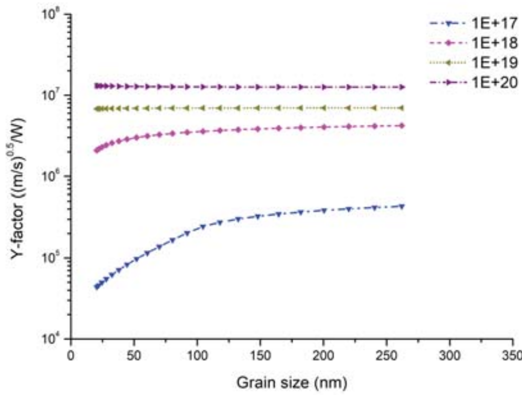

Fig. 6 The Y factor as a function of mean grain size for four different doping concentrations at $300K$ in p-doped polycrystalline silicon

V. Optimization of S Factor

There exists an optimized film thickness t_o for the S factor of thermopile sensor (7).

$$t_o = \frac{1.256}{\lambda} \tag{25}$$

with the best achievable structure factor of $S_o = 0.63817\sqrt{\lambda}$. Here the infrared absorption of passive support membrane and the surface reflection are neglected. Without external absorber the S factor vs. film thickness is shown in Fig.7. If infrared absorption coefficient λ is bigger, the optimized thickness is smaller. Normally the λ is small, thick film or multiple films should be used.

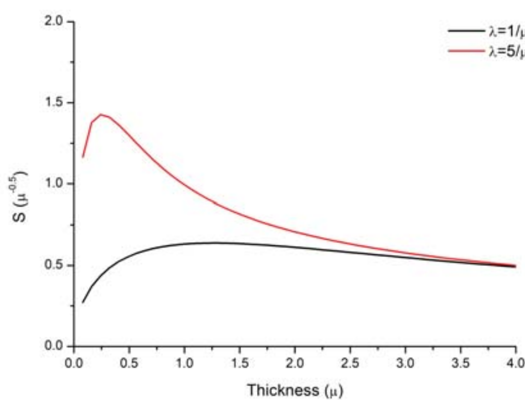

Fig. 7 The S factor as a function of film thickness for two absorption coefficients

VI. Optimization of Time Constant

It can be seen that for this simplified sensor model the specific detectivity is proportional to the square root of active area of sensor (9), whereas the time constant is proportional to the active area of sensor (16). The passive support membrane will increase the time constant. This also means that if an additional external absorber film is introduced, the dynamical behavior will be worse. Therefore, a compromise according to system specification of application should be made for sensor design.

VII. Optimization of G_f Factor

For infrared detection, large absorption coefficient λ is beneficial for specific detectivity (9). For thermopile sensor composed of parallel aligned identical rectangular thermopile strips with negligible gap between them and with one end on heat sink, the specific detectivity of $D^* = Y(1-R)l_i/\sqrt{t}$ can be obtained in the strong absorption limit, and $D^* = Y(1-R)l_i\lambda\sqrt{t}$ in the weak absorption limit. In these cases the D^* is independent of thermopile width and, thus, also independent of the number of thermopile strips.

For a real thermopile sensor design, where thermopile strips are assembled in a support membrane encompassed with heat sink, the G_f factor can be calculated with (8) or (11). Fig. 8 is a schematic layout of an idealized type I thermopile sensor on a square support membrane of size $a \times a$. The edges of membrane are connected to heat sink. For simplicity it is assumed that all thermopile strips have the same width, there are $4n$ strips, the corner with no thermopile strip has a size e, and the gap between neighboring strips is negligibly small. Since the thermal conductivity of passive materials used in the technology is much smaller than that of polycrystalline silicon, their contribution is negligible. The corner ratio is defined as $x = \frac{e}{a}$. The shape factor can be derived as

$$G_f = \begin{cases} \left(x^2 + x(1-2x)\frac{n^2-1}{2n^2} + (1-2x)^2\frac{n^2-1}{12n^2}\right) \\ \quad \cdot\sqrt{\frac{n^2(1-2x)}{n^2-1+2x(n^2+1)}} & n\,odd \\ \left(x^2 + \frac{1}{2}x(1-2x) + (1-2x)^2\frac{n^2+2}{12n^2}\right) \\ \quad \cdot\sqrt{\frac{1-2x}{1+2x}} & n\,even \end{cases} \tag{26}$$

The G_f factors as a function of corner ratio x for three different strip numbers n are shown in Fig. 9.

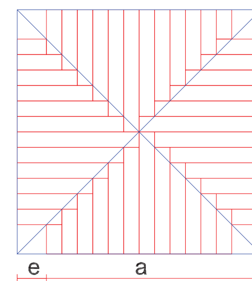

Fig. 8 The schematic layout of a type I thermopile sensor

Fig. 10 is a schematic layout of an idealized type II thermopile sensor on a square support membrane of size $a \times a$ with edges connected to heat sink. It is also assumed that all thermopile strips have the same width, there are $4n$ strips, the corner size is e, signal length is p, and the gap between neighboring strips is negligible. The corner ratio is also denoted as $x = \frac{e}{a}$, and the signal length ratio is defined as $y = \frac{p}{a}$. The shape factor is

Open Science Index, Materials and Metallurgical Engineering Vol:17, No:7, 2023 publications.waset.org/10013161.pdf

Open Science Index, Materials and Metallurgical Engineering Vol:17, No:7, 2023 publications.waset.org/10013161.pdf

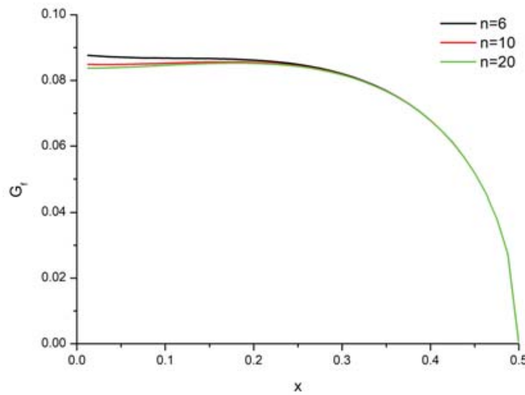

Fig. 9 The G_f factor of type I thermopile sensor as a function of corner ratio x for three different strip numbers

$$G_f = \begin{cases} \frac{\sqrt{y}}{2}((1+\frac{1}{n^2})x + \frac{n^2-1}{2n^2} - y) \\ \quad \cdot\sqrt{1-2x} & n\, odd \\ \frac{\sqrt{y}}{2}(x+\frac{1}{2}-y)\sqrt{1-2x} & n\, even \end{cases} \quad (27)$$

The G_f factors as a function of corner ratio x for three different signal length ratios are shown in Fig. 11a, while the G_f factors as a function of signal length ratio y for three different corner ratios are shown in Fig. 11b. Here the strip number is 4×20. As in the case of type I square sensor, it can be shown that the G_f factor depends only weakly upon the strip number.

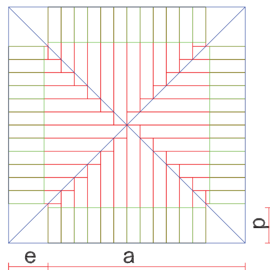

Fig. 10 The schematic layout of a type II thermopile sensor

If a type II sensor is realized on a circular support membrane of radius R, the schematic layout can be shown in Fig. 12. The signal length ratio is defined as $y = \frac{p}{R}$. The G_f factor as a function of signal length ratio y is shown in Fig. 13. For simplicity the gaps between the neighboring fan-shaped thermopile strips are also neglected here. For this idealized structure the shape factor is

$$G_f = \frac{2y - y^2}{2\sqrt{2\pi}\sqrt{-ln(1-y)}} \quad (28)$$

which is independent of strip number. The best signal length ratio is $y_o = 0.4665$, where the shape factor is $G_{fo} = 0.18$. This shows that the G_f factor of sensor on round support membrane can be much larger than the sensor realized on square support membrane.

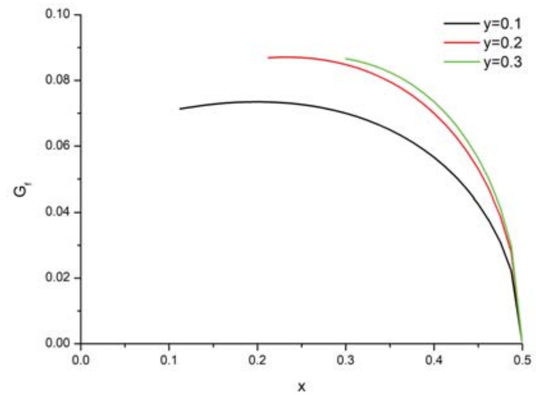

(a)

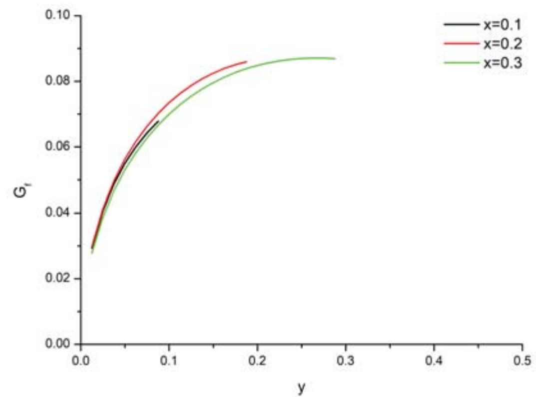

(b)

Fig. 11 The G_f factor of type II thermopile sensor: as a function of corner ratio x for three different signal length ratios (a), and as a function of signal length ratio y for three different corner ratios (b)

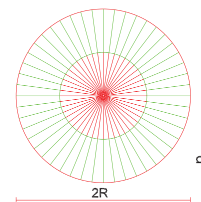

Fig. 12 The schematic layout of a circular type II thermopile sensor

The unitless G_f factors of different idealized sensor designs are discussed here. In real sensor design they will be reduced if the gaps of neighboring strips are not negligible, as will be shown in Table II.

VIII. Prototyping

Based on the theoretical analysis a prototype of thermopile infrared sensor of polycrystalline silicon on suspended support membrane is made. Because the infrared absorption coefficient of doped polycrystalline silicon film is about $\lambda = 10^4\, cm^{-1}$ [17], which is relative weak, a double layer polycrystalline

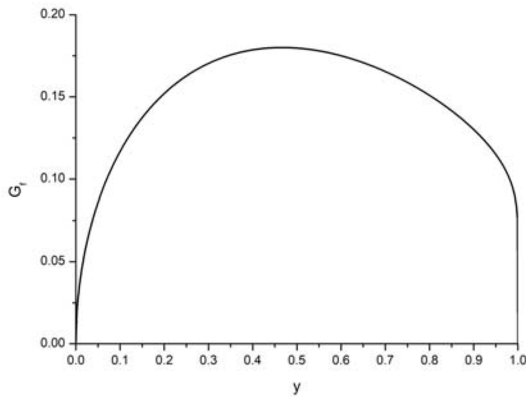

Fig. 13 The G_f factor of circular type II thermopile sensor as a function of signal length ratio y

Open Science Index, Materials and Metallurgical Engineering Vol:17, No:7, 2023 publications.waset.org/10013161.pdf

silicon technology is pursued to achieve a better S factor. The process steps are described below.

The 4-inch silicon substrate wafers are thermally oxidized with $300\,nm$ silicon dioxide, and CVD deposited $200\,nm$ silicon nitride film and $75\,nm$ silicon dioxide film as support membrane. Polycrystalline silicon film of thickness $430\,nm$ is thermally deposited ($600°C$). It is n-type doped with phosphorus oxychloride ($POCl_3$) deposition at $900°C$ for $40\,min.$ and annealed thereafter at $1110°C$ for $90\,min.$ in nitrogen gas. After a $100\,nm$ CVD silicon dioxide deposition as isolation film, a $300\,nm$ polycrystalline silicon film is deposited. The polycrystalline silicon film is thermally oxidized with $20\,nm$ silicon dioxide, afterward boron implant is made with implant energy $50\,keV$ and implant dose of $7 \times 10^{15}\,cm^{-2}$. After implant, the wafers are annealed at $1100°C$ for $30\,min.$ in nitrogen gas and passivated with $200\,nm$ thick silicon dioxide film. The support membrane is released from the substrate with KOH etching from back side. Contact pads are formed with $500\,nm$ Aluminum film (contained 1.2% Silicon). With the full process flow the doping concentration are determined with software Silvaco [18]. Simulation shows that the doping concentration of n-type polycrystalline silicon film is $1.3 \times 10^{20}\,cm^{-3}$ phosphorus, that of p-type polycrystalline silicon film is $6.7 \times 10^{19}\,cm^{-3}$ boron. The room temperature electrical sheet resistivity measured for n- and p-type polycrystalline silicon are $20.8\,\Omega/\square$ and $127.2\,\Omega/\square$, respectively. This agrees with the model calculation. Scanning electron microscope measurement (SEM) showed that the grain sizes are from $100\,nm$ to $200\,nm$. The measured technology parameters together with the simulated Y factors are listed in Table I.

Two different kinds of thermopile sensors have been designed for this prototyping. One is type I sensor chip I (Fig. 14), which is similar to the ideal structure of Fig. 8. The other is type II sensor chip II (Fig. 15), which is similar to the ideal structure of Fig. 10. Both have an active area of $1.2\,mm \times 1.2\,mm$. From (8) and (11), the G_f factors of the real sensors are calculated for n- and p-type polycrystalline silicon films and listed in Table II. Specific detectivities for each polycrystalline silicon film of two sensors are calculated with Y factors in Table I. The total sensor specific detectivity D^* is the sum of D^* from n- and p-type polycrystalline silicon films. They agree well with the measured values, which are characterized with high temperature black body calibration source (Table II). This means that the deviation due to the effect of isolation and passivation layers and support membrane is small. On the other hand, one can see that the realized G_f factor is smaller than that of ideal structure. The smaller G_f factor is due to the big thermopile strip separation and overlap used in prototyping design.

The measured time constant for both sensors is $7.6\,ms$, which agrees with (16).

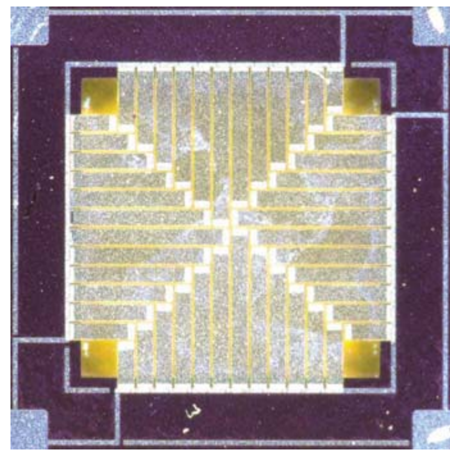

Fig. 14 Thermopile sensor chip I

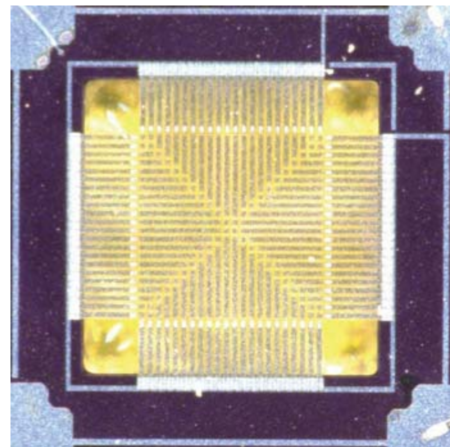

Fig. 15 Thermopile sensor chip II

IX. Summary and Discussion

In this article, an approach is presented for the optimization of thermopile performance. The two dimensional temperature distribution of thin film is utilized to decouple the sensor performance according to the contributions of material thermoelectric properties, layer structure, and sensor geometry contributions. It is shown that the specific detectivity can be

TABLE I
THERMOELECTRIC PROPERTIES OF POLYCRYSTALLINE SILICON FILM

Polysilicon	Thickness	Grain size	Sheet resist	Y factor
	nm	nm	$\Omega/\square$	$(cm/s)^{0.5}/W$
n	430 ± 5	220 ± 90	20.8 ± 0.3	1.9E8
p	300 ± 4	120 ± 40	127.2 ± 1.6	1.2E8

TABLE II
G_f FACTOR AND SPECIFIC DETECTIVITY

Sensor	Type	$G_f(n)$	$D^*(n)$	$G_f(p)$	$D^*(p)$	$D^*(sim.)$	$D^*(exp.)$
			$cm(Hz)^{0.5}/W$		$cm(Hz)^{0.5}/W$	$cm(Hz)^{0.5}/W$	$cm(Hz)^{0.5}/W$
TP11	I	0.079	9.75×10^7	0.072	4.70×10^7	1.44×10^8	1.17×10^8
TP12	II	0.071	8.87×10^7	0.058	1.27×10^7	1.27×10^8	1.09×10^8

Open Science Index, Materials and Metallurgical Engineering Vol:17, No:7, 2023 publications.waset.org/10013161.pdf

well simplified as the product of Y factor, S factor, G_f factor and square root of active area A.

Based on the relaxation times of phonon and charge carrier scattering, the thermal conductivity, electrical conductivity, and Seebeck coefficient can be calculated. This approach includes most of the important effects of phonon and charge carrier scattering at impurities, grain boundaries and grain boundary traps. The effect of grain boundary traps induced reduction of charge carrier concentration is also taken into account. Although phonons and charge carriers contribute very differently to thermoelectric-based infrared detection, the optimization of thermoelectric material properties can be subsumed in the optimization of a single Y factor. The effects of doping concentration, grain size and trap density on the Y factor are systematically discussed for temperatures close to room temperature. In agreement with experiments, it is shown that heavily doped polycrystalline silicon film with a mean grain size of approximately $100\,nm$ can achieve a Y factor comparable to that of crystalline silicon film. This is quite different to infrared sensors based on the photovoltaic effect, in which case sensors made of a polycrystalline material exhibit deficient performance compared with those made of a crystalline material. Physically, this is due to the fact that excess phonon scattering can outperform charge carrier scattering in case of polycrystalline film. Although the Y factor of polycrystalline silicon is only slightly better than that of crystalline silicon, very thin film can be easily realized with polycrystalline silicon deposition on oxidized silicon substrate and a subsequent substrate etching. This is crucial for the high thermal resistance needed for infrared sensor.

The S factor is correlated with infrared absorption coefficient. If the film thickness is not so thick that the two dimensional temperature distribution supposition is no more correct, the optimized film thickness is anti proportional to the absorption coefficient. For strong infrared absorption thinner film is preferred. For weak infrared absorption, multilayer structure technology should be utilized to improve the sensor performance and compensate the film eigenstrain simultaneously. For sensor made from homogeneous material time constant is proportional to the sensor active area. The time constant is larger for smaller thermal conductivity and bigger thermal capacitance. The time constant can be effectively reduced with smaller active sensor area.

From the prototyping it can be seen that the effect of geometry layout can be described well by the G_f factor for thin film sensor. This is due to the small thermal conductivity of supporting membrane and isolation and passivation layers, so that the heat flows mainly along the thermopile strips. Therefore, the one dimensional approximation can describe the real temperature profile in each thermopile strip well. It can also be seen that sensor on round support membrane has much larger G_f factor than sensor on square support membrane. For the two type of chips on square membrane, although the G_f factor can be improved by reducing the thermopile strip overlaps and separations, the best achievable G_f factors are comparable. Numerical calculation shows that this is also the case if the widths of different thermopile strips can be randomly changed.

The approach presented herein can be extended to investigate the optimization of thermopile sensors based on other crystalline and polycrystalline semiconductors.

ACKNOWLEDGMENT

We thank Mr. Geert Brokmann for the valuable discussions and suggestions.

REFERENCES

[1] C. Goupil, W. Seifert, K. Zabrocki, E. Müller, and G. J. Snyder, “Thermodynamics of thermoelectric phenomena and applications,” *Entropy*, vol. 2011, no. 13, pp. 1481–1516, Aug. 2011.

[2] A. Graf, M. Arndt, and G. Gerlach, “Seebeck’s effect in micromachined thermopiles for infrared detection. A review,” *Proc. Estonian Acad. Sci. Eng.*, vol. 13, no. 4, pp. 338–353, June 2007.

[3] U. Dillner, E. Kessler, and H. G. Meyer, “Figures of merit of thermoelectric and bolometric thermal radiation sensors,” *J. Sens. Sens. Syst.*, vol. 2, no. 1, pp. 85–94, June 2013.

[4] H. Zhou, P. Kropelnicki, J. M. Tsai, and C. Lee, “Development of a thermopile infrared sensor using stacked double polycrystalline silicon layers based on the CMOS process,” *J. Micromech. Microeng.*, vol. 23, no. 6, p. 065026, May 2013.

[5] H. B. Callen, “The application of Onsager’s reciprocal relations to thermoelectric, thermomagnetic, and galvanomagnetic effects,” *Phys. Rev.*, vol. 73, no. 11, pp. 1349–1358, Jun. 1948.

[6] N. C.-C. Lu, L. Gerzberg, C.-Y. Lu, and J. D. Meindl, “Modeling and optimization of monolithic polycrystalline silicon resistors,” *IEEE Transactions on Electron Devices*, vol. ED-28, no. 7, pp. 818–830, Jul. 1981.

[7] J. Y. W. Seto, “The electrical properties of polycrystalline silicon films,” *J. Appl. Phys.*, vol. 46, no. 12, pp. 5247–5254, Dec. 1975.
[8] A. D. McConnell, S. Uma, and K. E. Goodson, “Thermal conductivity of doped polysilicon layers,” *J. MICROELECTROMECHANICAL SYSTEMS*, vol. 10, no. 3, pp. 360–369, Sep. 2001.
[9] N. Neophytou, X. Zianni, H. Kosina, S. Frabboni, B. Lorenzi, and D. Narducci, “Simultaneous increase in electrical conductivity and seebeck coefficient in highly boron-doped nanocrystalline Si,” *Nanotechnology*, vol. 24, no. 20, p. 205402, May 2013.
[10] A. C. Sparavigna, “The boltzmann equation of phonon thermal transport solved in the relaxation time approximation - I - Theory,” *Mechanics, Materials Science & Engineering*, vol. 2016, no. 3, pp. 34–45, Mar. 2016.
[11] C. B. Vining, “A model for the high-temperature transport properties of heavily doped n-type silicon-germanium alloys,” *J. Appl. Phys.*, vol. 69, no. 1, pp. 331–341, Jan. 1991.
[12] L. Long and T. Ortlepp, “Thermoelectric properties of doped polycrystalline silicon film,” *This proceeding*, July 2022.
[13] M. G. Holland, “Analysis of lattice thermal conductivity,” *Phys. Rev.*, vol. 132, no. 6, pp. 2461–2471, Dec. 1963.
[14] J. Y. W. Seto, “Deposition of polycrystalline silicon by pyrolysis of silane in argon,” *J. Electrochem. Soc.: Solid-State Science and Technology*, vol. 122, no. 5, pp. 701–706, May 1975.
[15] B. P. Tyagi and K. Sen, “Electrical properties of polycrystalline silicon in the dark and under illumination,” *phys. stat. sol. (a)*, vol. 90, no. 2, pp. 709–713, Aug. 1985.
[16] N. C.-C. Lu, L. Gerzberg, C.-Y. Lu, and J. D. Meindl, “A conduction model for semiconductor-grain-boundary-semiconductor barriers in polycrystalline-silicon films,” *IEEE Transactions on Electron Devices*, vol. ED-30, no. 2, pp. 137–149, Feb. 1983.
[17] M. Tuohiniemi, M. Blomberg, and F. Gao, “Infrared spectroscopy study of a poly-silicon film for optimizing the boron-implanting dose,” *JOURNAL OF MICROELECTROMECHANICAL SYSTEMS*, vol. 22, no. 5, pp. 1207–1212, Oct. 2013.
[18] Silvaco, *Athena user’s manual*. Santa Clara, CA 95054: Silvaco, Inc, 2015.

Open Science Index, Materials and Metallurgical Engineering Vol:17, No:7, 2023 publications.waset.org/10013161.pdf

Li Long received the B.S. and M.S. degrees in Physics from Wuhan University, P.R. China, in 1983 and 1986, respectively, and the Ph.D degree in Physics from Technische Universität Bergakdemic Freiberg, Germany, in 2001. From 1986 to 1995 he was a lecturer at the Physics department, Wuhan University, P. R. China. From 2001 to 2002 he was a postdoc at the Faculty of Physics, Universität Halle, Germany. In 2003 he was a postdoc at the Max Planck Institute of microstructure physics, Halle, Germany. Since 2004 he has been an R&D engineer and project leader at the CiS Research Institute of Microsensors, Erfurt, Germany. His research focuses on the development of silicon microsensors. His work includes design, simulation, and analysis of thermopile sensors, photosensors, micro-strip detectors and micro-pixel detectors.

Thomas Ortlepp was born in Friedrichroda, Thuringia, in 1972 and is a trained maintenance mechanic. He studied mathematics at the Technical University of Ilmenau and received his PhD in quantum electronics in 2004. After that, Thomas Ortlepp did research in the field of low-temperature physics at the University of Twente in Holland. In 2010, Thomas Ortlepp habilitated in the field of microelectronics and subsequently took over the leadership of an industrial project for high-performance quantum memory circuits at the University of Berkeley in California. In 2013, Thomas Ortlepp returned to Germany and started his career at CiS Forschungsinstitut für Mikroelektronik GmbH. In 2015, he was appointed Distinguished Professor by Yokohama National University. Also in 2015, Thomas Ortlepp took over the management of the CiS Research Institute of Microsensors (CiS Forschungsinstitut für Mikroelektronik GmbH) until today. He is co-founder and vice president of the MEMS Smart Sensor Institute in Nanjing, China, which was established in 2018. His research focuses on the development of silicon microsystems (MEMS and MOEMS) and the industrial application of quantum technology.